



# Application of micro-computed X-ray tomography for improving the hole erosion test analysis on high plastic clay

Bahaeldeen Zaid<sup>1</sup> · Florian Vollert<sup>2</sup> · Jens Gibmeier<sup>2</sup> · Lena Mengel<sup>1</sup> · Oliver Stelzer<sup>1</sup> · Achim Schneider<sup>1</sup>

Received: 9 February 2022 / Accepted: 21 May 2022  
© The Author(s) 2022

## Abstract

The hole erosion test (HET) was developed to simulate piping erosion and to study the erosion parameters of cohesive soils. The erosion rate in the HET is evaluated by the enlargement of a pre-performed hole in the axis of the specimen with time. The hole diameter during the test is estimated using the pipe flow theory with an assumption that the friction factor varies linearly with time. To investigate this assumption, measurements of the hole diameter during the test are needed. So far, there have been no measurements of the hole diameter during the HET and the hole diameter is measured only at the end of the test after cutting the specimen. In this study, a novel approach to measure the hole diameter at different time steps during the HET using micro-computed X-ray tomography ( $\mu$ CT) is presented. Combining the HET and  $\mu$ CT data, the assumption regarding the friction factor was investigated. Moreover, a linear relation between the flow rate and the hole diameter was found in the range of the tested diameters. This relation was confirmed with HETs using non-erodible PVC specimens with different hole diameters. Accordingly, a new method to interpret the HET for high plastic clay was proposed, in which the hole diameter is calculated based on the flow rate, given that the initial and the final hole diameters are known. A comparison between the analysis of the HET using the proposed and the previous analysis methods is presented.

**Keywords** Computed X-ray tomography · Erosion parameters · High plastic clay · Hole erosion test

## 1 Introduction

The hole erosion test (HET) was developed by Wan and Fell [21] to simulate piping erosion and to evaluate the erosion parameters of cohesive soil. The HET was confirmed to be an excellent tool in quantifying the rate of erosion in concentrated leak in a soil [3]. Over time, the HET was subjected to many modifications and improvements in the test setup and the test interpretation [4–6, 8, 11, 12, 14, 16, 23]. In the HET a soil is compacted inside a standard compaction test mould and an axial hole is drilled along the soil specimen. The flow through the hole in the specimen is driven by a head difference between a high-level tank upstream the specimen and a low-level

tank downstream of it. The flow through the hole causes the hole diameter to increase with time due to the erosion process. The flow rate and the hydraulic head difference between upstream and downstream of the specimen are measured during the test. The final hole diameter is measured at the end of the test using, for example, a plaster cast of the hole.

By applying a force balance on a volume of fluid in a pipe in the direction of flow, the shear stress acting on the hole boundary can be expressed as shown in Eq. 1.

$$\tau_b = \rho_w g \frac{\Phi \Delta h}{4 L} \quad (1)$$

where  $T_b$  is the hydraulic shear stress ( $\text{N/m}^2$ ),  $\phi$  is the hole diameter (m),  $\Delta h$  is the hydraulic head difference between upstream and downstream the specimen (m),  $L$  is the length of the specimen (m),  $\rho_w$  is the water density ( $\text{kg/m}^3$ ) and  $g$  is the acceleration of gravity ( $\text{m/s}^2$ ). Since the flow in the HET is turbulent [2], the hole diameter ( $\phi_t$ ) at time  $t$  during the test is estimated using Eq. 2 for turbulent flow condition [21].

✉ Bahaeldeen Zaid  
bahaeldeen.zaid@baw.de

<sup>1</sup> Geotechnical Department, Federal Waterways Engineering and Research Institute (BAW), Karlsruhe, Germany

<sup>2</sup> Institute for Applied Materials (IAM-WK), Karlsruhe Institute of Technology (KIT), Karlsruhe, Germany

$$\Phi_t = \left( \frac{64Q_t^2 f_{Tt}}{\pi^2 \rho_w g \frac{\Delta h_t}{L}} \right)^{1/5} \quad (2)$$

where  $Q_t$  is the flow rate ( $\text{m}^3/\text{s}$ ),  $f_{Tt}$  ( $\text{kg}/\text{m}^3$ ) friction factors linking the shear stress to the mean flow velocity. The friction factor at the beginning and at the end of the test can be calculated since the initial hole diameter is known and the final hole diameter can be measured at the end of the test. During the test, the friction factor is assumed to vary linearly with time [21]. However, Lim [10] found that the friction factor does not vary linearly with time, rather with hole diameter and flow rate. Wahl et al. [20] found a linear relation between friction factor and hole diameter and a linear trend between friction factor and time but only with a low coefficient of determination  $R^2$ . The linearity between friction factor and hole diameter according to Lim [10] was applied by Khoshghalb et al. [9] in the analysis of the HET. However, Lim [11] and Wahl et al. [20] carried out several HETs on different specimens, where they stopped the HETs at different flow rates and measured the hole diameter at the end of each test. They calculated the initial and final friction factors for each test and plotted them against, for example, the hole diameter. In this way, the friction factors were calculated for different specimens in which the preparation of the specimens could result in some differences in the specimen properties and the erosion process. In the present study, the friction factor was investigated in the same specimen using  $\mu\text{CT}$ -scan.

The erosion rate per unit surface area of the hole is calculated using Eq. 3.

$$\dot{\varepsilon} = \frac{\rho_d}{2} \frac{d\phi}{dt} \quad (3)$$

where  $\phi$  is the hole diameters (m),  $t$  is the time (s) and  $\rho_d$  is the dry density of the soil ( $\text{kg}/\text{m}^3$ ).

By plotting the erosion rates against the hydraulic shear stresses, a nearly linear relationship is obtained, which is used to determine the erosion characteristics of the soil [7, 21]. Wan and Fell [21] defined the slope of the line of best fit in the aforementioned relation as the coefficient of soil erosion  $C_e$  and proposed the erosion rate index  $I$  to be calculated as shown in Eq. 4.

$$I = -\log(C_e) \quad (4)$$

Wan and Fell [21] classified the soil based on the erosion rate index into six categories, from extremely rapid erodible soil at  $I < 2$  to extremely low erodible soil for  $I > 6$ .

In this study,  $\mu\text{CT}$  was used to investigate the assumption regarding the friction factor, which is necessary to interpret the HET. Furthermore, based on the results of the  $\mu\text{CT}$ , a proposed method for interpreting the HET for high plastic clay is introduced. Finally, the proposed and

previous interpretation methods were applied to a HET and the results were compared.

## 2 Experiments and methods

### 2.1 Hole Erosion test

#### 2.1.1 Device setup

A modified hole erosion test developed at the German Federal Waterways Engineering and Research Institute [8] on the basis of HET-P [12] was used in this study (Fig. 1). The specimen cylinder is made of Plexiglas and has an internal diameter of 7.8 cm and a length of 12.8 cm. The length of the Plexiglas pipe upstream and downstream the specimen is 40 and 60 cm, respectively. The head difference between high-level tank and low-level tank is adjustable and can reach 2.9 m. The flow through the specimen is driven by a constant head difference between the high-level and the low-level tanks. A differential pressure sensor was used to measure the pressure difference between upstream ( $h_u$ ) and downstream ( $h_d$ ) the specimen. The flow rate was measured downstream the specimen using a magnetic-inductive flowmeter (MID). The vertical alignment of the device helps producing a symmetrical hole and prevent accumulation of the eroded material in the hole [5].

A collecting tank downstream the low-level tank was installed with a pump to recirculate the water back to the high-level tank and to collect the overflow from the high-level tank.

#### 2.1.2 Test material

Two high plastic clays, namely Nottenkaemper (NTK) clay and Hohenwarsleben (HWL) clay, were used in the HETs. The grain size distribution of NTK and HWL is shown in Fig. 2. The characteristics of each clay type are shown in Tables 1 and 2. Both clay types are typically used as sealing material in the waterways in Germany, more specific for canals, which are built above the ground water level (Fig. 3). Due to ship-induced hydraulic actions on the sealing and possible damages caused by plant roots, the erosion resistance of the clay needs to be investigated.

In addition, four PVC specimens (Fig. 1b) with different diameters (9, 12, 16 and 30 mm) were used to investigate the relationship between the hole diameter and the flow rate in the HET.

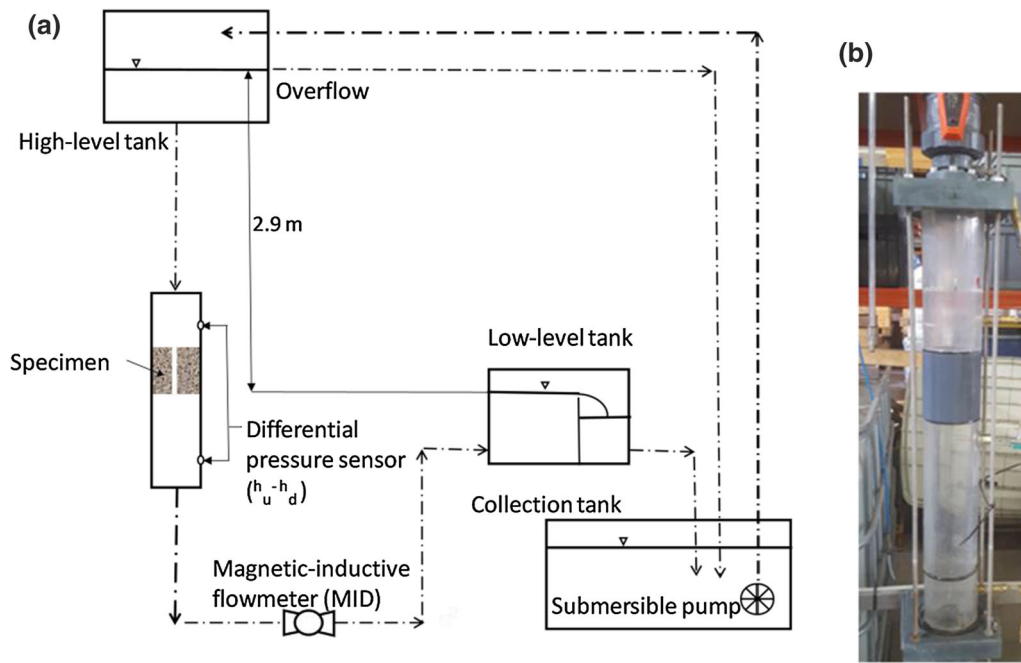


Fig. 1 Hole erosion test device: a device setup; b device photo with a PVC specimen

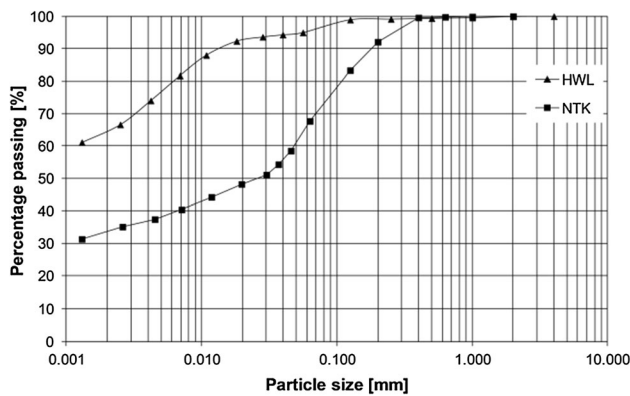


Fig. 2 Grain size distribution of NTK and HWL

Table 1 Properties of Nottenkaemper (NTK) and Hohenwarsleben (HWL) clay samples

Parameters		Clay type	
		NTK	HWL
Clay content ( $d < 2 \mu\text{m}$ )	[%]	34 – 42	60 – 64
Silt	[%]	34 – 54	29 – 35
Sand	[%]	12 – 24	5 – 7
Liquid limit	[%]	58.2	65.0
Plasticity	[%]	35	42
Preparation water content (Water content at undrained shear strength $c_u = 20 \text{ kPa}$ )	[%]	27	40
Density	$\text{kg}/\text{m}^3$	1930	1798

Table 2 Clay mineral content [%]

Material	Clay type	
	NTK	HWL
Kaolinite	8	27
Illite	22	22
Smectite	3	
Chlorite	6	
Quartz	46	
Albite	1	
Microcline	2	
Calcite	7	9.2
Gypsum	3	2.4
Organic content	< 1	
Pyrite		< 0.1
Dolomite		< 0.5
Montmorillonite		7
Organic content	< 1	
Rest (Quartz + organic + Feldspar)		31.8

### 2.1.3 Specimen preparation

The soil was compacted inside the specimen cylinder. The specimen was prepared in three layers each one compacted using Proctor hammer (Fig. 4a).

The specimens were prepared at an undrained shear strength  $c_u = 20 \text{ kPa}$  which is required for the installation



**Fig. 3** Installation of a sealing clay layer under water condition (BAW Image archive)

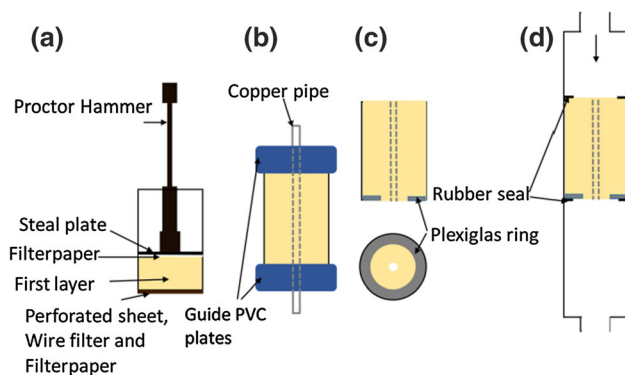


**Fig. 4** Schematic representation of the specimen preparation: **a** layer compaction; **b** preparation of the hole; **c** anti-slip support; **d** installation of the specimen cylinder in the test chamber

of the clay layers under water condition according to the guidelines of the Federal Waterways Engineering and Research Institute. A Laboratory vane shear apparatus was used to determine the water content required to arrive at  $c_u = 20$  kPa. The hole was introduced by inserting the copper pipe by hand through the soil. Two guide PVC plates were used to ensure the accuracy while inserting the copper pipe in the specimen (Fig. 4b). Before installing the specimen cylinder in the specimen chamber (Fig. 4d), a Plexiglas ring is installed beneath the specimen to avoid sliding of the specimen during the test (Fig. 4c).

#### 2.1.4 Test programme and procedure

Two HETs were conducted to investigate the relationship between friction factor and hole diameter, flow rate and time as well as the relation between hole diameter and flow rate. Two specimens, one obtained from NTK clay and the other one from HWL clay, were used in the tests. The two HETs were combined with  $\mu$ CT for measuring the hole diameter several times during the test in an interrupted test

run, i.e. the HET was paused after a preset time and the specimen cylinder was dismantled and transported to the  $\mu$ CT (Sec. 2.2.2) for measuring the hole diameter. After performing the  $\mu$ CT-scan, the specimen cylinder was installed again in the HET device and the test was continued to the next stop point. At the end of the HET gypsum was poured inside the hole to get the hole plaster cast, which was subsequently scanned using photogrammetry (Artec 3D Scanner, Sec. 2.2.1) to capture the hole geometry (Fig. 6). The results of the photogrammetry scan were compared with the  $\mu$ CT results (Sec. 2.2.2). To investigate further the relationship between the flow rate and the hole diameter, four HETs were carried out on the four PVC specimens (Sec. 2.1.2). The flow rate in each test was measured using a magnetic-inductive flowmeter (MID). Since the hole diameters of the PVC specimens are known, the relationship between the hole diameter and the flow rate was established (Sec. 3.4) and a proposed method for interpreting the HET was introduced. One HET on NTK clay was performed to compare the analysis of HET using the proposed and the previous interpretation methods. The boundary flow condition in all HETs was kept constant (head difference of 2.9 m).

#### 2.1.5 Estimation of the friction factor

The estimation of the friction factor is essential for the interpretation of the HET. The friction factor is usually divided into skin friction (grain friction) and form friction [1, 2, 24]. The irregularities in the HET may increase the contribution of the form friction. However, the role of these two kinds of friction on cohesive soils as well as in pipe flow is not fully understood [2]. The investigations herein address how the friction factor develop during a HET test.

The friction factors  $f_{Tl}$  can be calculated using Eq. 2. Instead of  $\Delta h$ , the effective hydraulic head difference  $\Delta h_{eff}$  was used to account for the entrance and exit losses. Equation 5 is used to calculate the effective hydraulic head difference. Considering that the edge of the hole at the entrance is quickly rounded after the start of the test, the entrance losses coefficient  $K_{Ent}$  can be taken as 0.05 [22]. The exit losses can be estimated using Eq. 6 [22]. The consideration of the local head losses was highlighted in different studies [2, 11, 13, 17]. Neglecting the local head losses results in significantly overestimating the hydraulic shear stress.

$$\Delta h_{eff} = h_u - h_d - \left[ K_{Ent} \frac{v^2}{2 \cdot g} + K_{Ext} \frac{v^2}{2 \cdot g} \right] \quad (5)$$

where  $K_{Ent}$  and  $K_{Ext}$  are the entrance and the exit losses coefficient, respectively, and  $h_u$  and  $h_d$  are the hydraulic head upstream and downstream the specimen, respectively.

$$K_{\text{Ext}} = \left[ 1 - \frac{\phi_h^2}{\phi_p^2} \right]^2 \quad (6)$$

where  $\phi_h$  is the hole diameter [m] and  $\phi_p$  is the pipe diameter downstream the specimen [m].

## 2.2 Measurement of the hole diameter

The determination of the final hole diameter is very important for the interpretation of the HET. However, difficulties in determining the hole diameter arise when the hole size is not uniform throughout the hole length. Different methods were applied to measure the final hole diameter. Lim [10] cut the specimen in three location and directly measured the hole diameter with a calliper. Using a plaster cast of the hole similar to that in Fig. 6a, more direct measurements of the hole diameter were taken with the calliper [11, 20]. The measurement of the hole diameter with the calliper may incorporate some inaccuracies, considering that the shape of the hole, in many cases, is not perfectly circular. Haghighi et al. [6] poured molten paraffin into the eroded hole and used the volume of the paraffin after it solidifies to calculate the hole diameter. In this paper, two methods were used to measure the hole geometry of the clay specimens, namely  $\mu$ CT-scan and photogrammetric 3D scanning of the hole plaster cast.

### 2.2.1 Micro-computed X-ray tomography ( $\mu$ CT)

The  $\mu$ CT-scans were performed on two clay specimens (4 scans on the NTK clay specimen and 5 scans on the HWL clay specimen). The samples were properly sealed with plastic foil and two plastic covers at both sides to avoid changes in the water content of the specimens (Fig. 5a). The  $\mu$ CT-scans were carried out using the YXLON CT Precision computed tomography system. The parameters of the  $\mu$ CT-scan are shown in Table 3. For the investigated specimen, the reflection tube head Y.FXE 225.48 with an acceleration voltage of 170 kV and a current of 0.2 mA was chosen. The specimen (Fig. 5a) was positioned on the

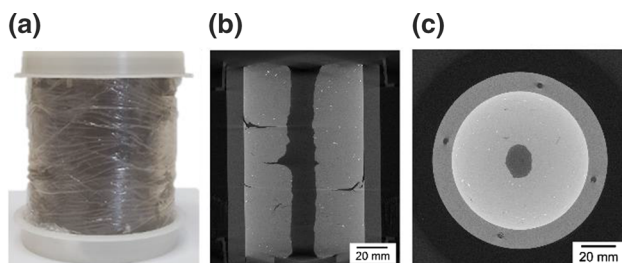


**Fig. 5**  $\mu$ CT-scan No. 4 on NTK: **a** specimen photo; **b**  $\mu$ CT projection of the vertical cross section; **c**  $\mu$ CT projection of the horizontal cross section

**Table 3**  $\mu$ CT-scan parameters for the investigated sample

Tube head	Reflection
Acceleration voltage	170 kV
Tube current	0.2 mA
Focus-sample distance	321.43 mm
Sample-detector distance	578.57 mm
Voxel size	71.43 $\mu$ m
Detector edge length	409.6 mm
Number of detector pixels	2048
Integration time	1000 ms
Number of projections	2400

rotatable plate between tube and detector with a focus-sample distance of 321.43 mm and a sample-detector distance of 578.57 mm. The resulting cubic voxel size of the reconstructed images is 71.43  $\mu$ m. This allowed to fit the entire specimen in one image (Fig. 5b, c). At defined rotation angles, 2400 projection images were acquired by the detector. From these two-dimensional projection images, a volumetric image of the sample was reconstructed, which allows the visual inspection of the hole with sectional images.

The reconstructed sectional images of the specimen were evaluated using the open-source software ImageJ [18, 19]. Using this software, the images were segmented in order to subdivide the voxels in two areas: “hole” and “material”. For this purpose, the thresholding algorithm following Otsu [15] was applied. Afterwards, the acquired binary images were evaluated to determine the area of the hole over the height of the specimen at spacing of the voxel size. The equivalent hole diameter at each height  $\phi_h$  was calculated over the specimen height from the determined hole area at each height  $A_h$  using Eq. 7.

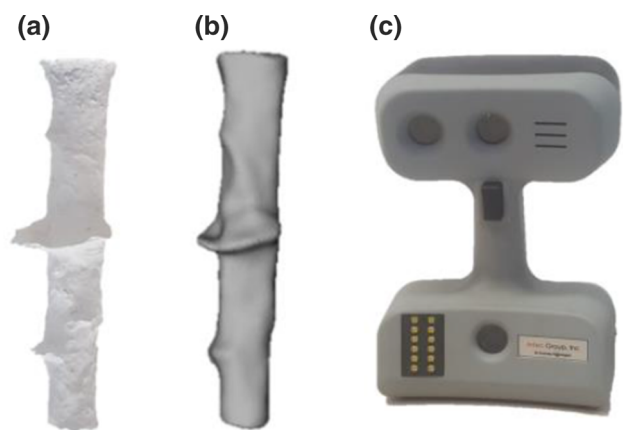


**Fig. 6** Photogrammetric 3D scanning of the hole plaster cast: **a** photo of the plaster cast of the hole; **b** 3D model of the hole plaster cast; **c** Artec MHT 3D Scanner

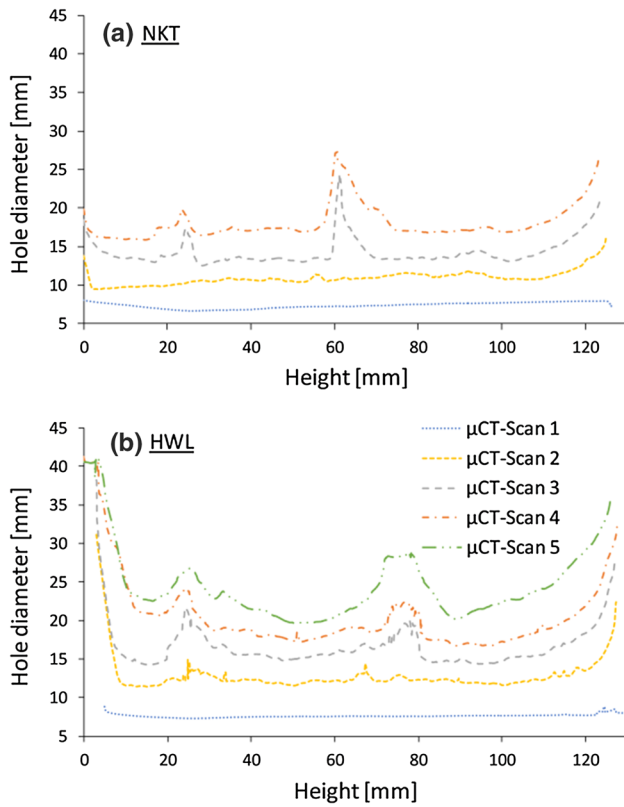


**Fig. 7** Hole diameter over the specimen height: **a** NTK clay specimen, to the right selected projection images for weak area in the specimen causing spikes in the hole diameter as the HET progresses; **b** HWL clay specimen

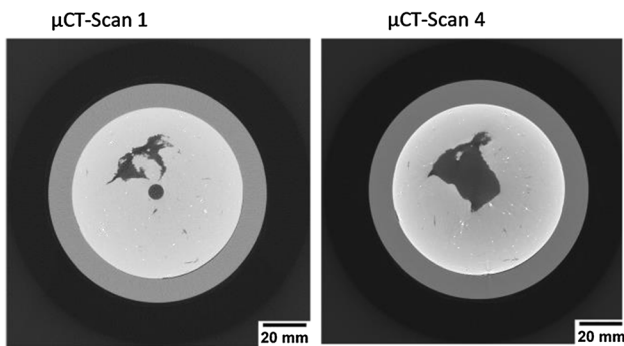


**Fig. 8** Projection  $\mu$ CT-scan images for weak area in NTK specimen at height of approx. 60 mm at the begging and at the end of the HET

$$\phi_h = \sqrt{\frac{4A_h}{\pi}} \quad (7)$$

The hole diameter was averaged over the specimen height to get hole diameter, which was used in the analysis of the HET.

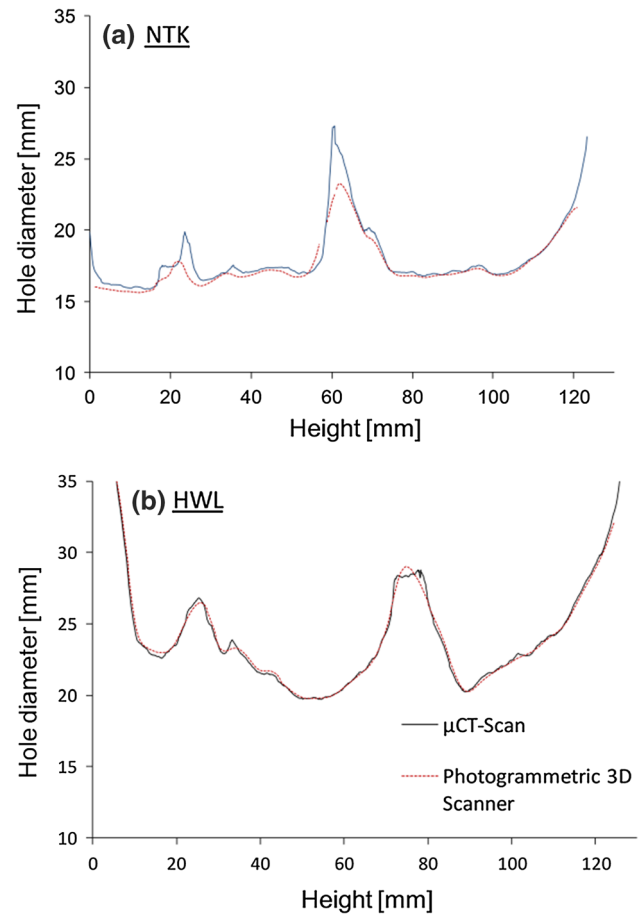


**Fig. 9** Final hole diameter over the height of the specimens measured using  $\mu$ CT-scan and the photogrammetric 3D scanner: **a** NTK clay specimen; **b** HWL clay specimen

## 2.2.2 Photogrammetric 3D scanning of the hole plaster cast

The hole diameter was measured at the end of the HET using a 3D scanner in order to confirm the accuracy of the  $\mu$ CT-scan.

The hole plaster cast was scanned using a professional handheld photogrammetric 3D scanner (Artec MHT 3D scanner). The plaster cast of the hole (Fig. 6a) was set on a rotating table and the 3D scanner (Fig. 6c) was oriented at the plaster cast and fixed while scanning. The photogrammetry scans were carried out from a distance of about 0.5 m to the plaster cast resulting in a nominal accuracy of about 0.1 mm.

Using the 3D model of the hole (Fig. 6b), the cross-sectional area of the hole  $A_h$  at different heights was calculated with the scanner's software. The hole diameter  $\phi_h$  at height  $h$  of hole is calculated using the area  $A_h$  as shown in Eq. 7.

The final hole diameter is calculated as the average diameter over the height of the hole.

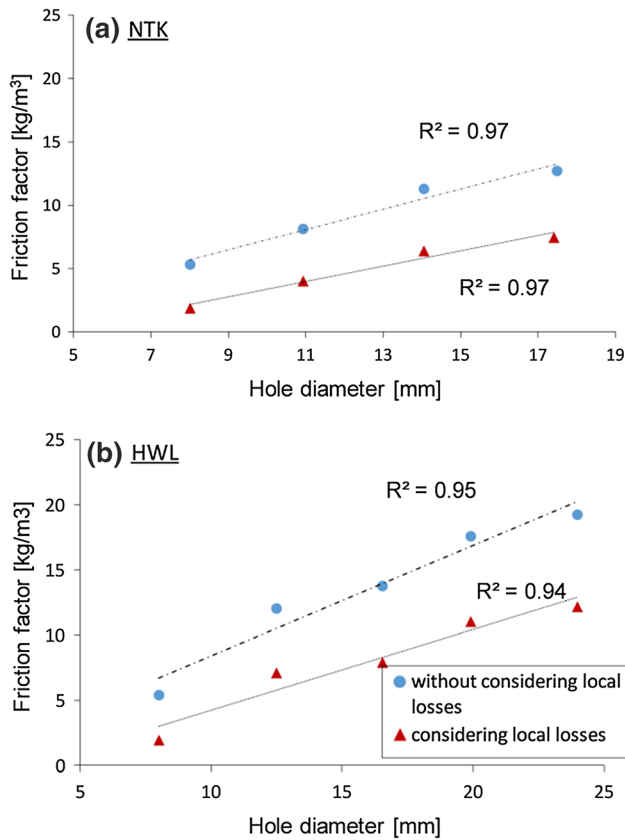


**Fig. 10** Relationship between the friction factor and the hole diameter: **a** for NTK clay; **b** for HWL clay

### 3 Results and discussion

#### 3.1 Hole diameter

Using the  $\mu$ CT-scan, the hole diameter was determined at different time intervals for NKT clay and HWL clay. The hole diameter over the specimen height for different  $\mu$ CT-scans is shown in Fig. 7. The final hole diameter for each scan was calculated as the average diameter over the specimen height. The  $\mu$ CT-scan analysis allowed identifying some weak areas in the specimen, which causes irregularities in the geometry of the hole. Figure 8 shows trapped air in the specimen, i.e. voids in the first scan ( $\mu$ CT-scan 1) at a height of about 60 mm of the specimen. While the hole diameter increased in the HET, the voids were connected to the hole causing large local erosion and large hole diameter see  $\mu$ CT-scan 4 in Fig. 8. The large hole diameter at the weak areas was excluded when calculating the average hole diameter.

To confirm the accuracy of the  $\mu$ CT-scans, the results of the  $\mu$ CT-scan at the end of the HET was compared with the results of the photogrammetric 3D Scanner (Fig. 9). A good agreement between the hole diameter measured using the  $\mu$ CT and the photogrammetric 3D Scanner was found.

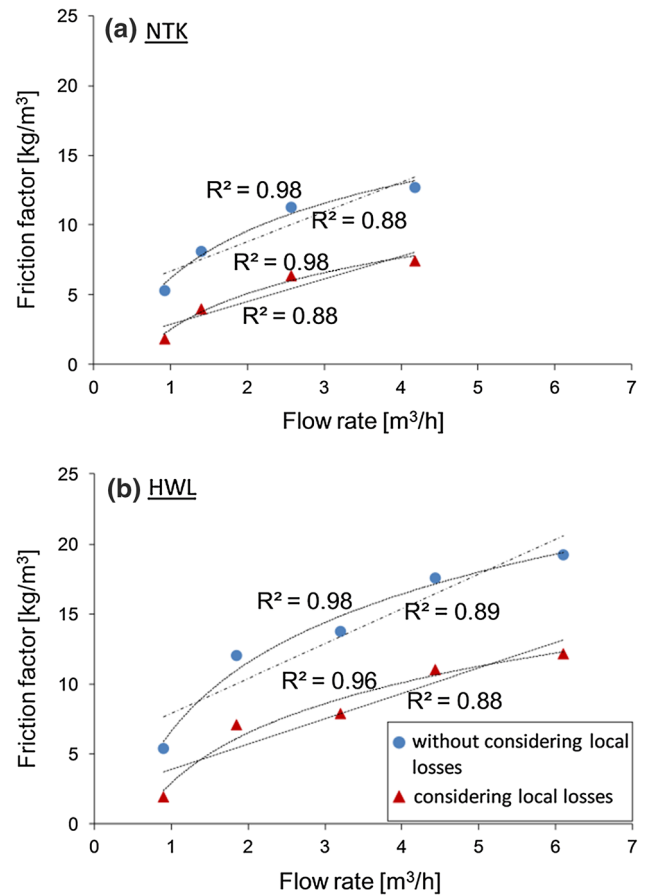


**Fig. 11** Correlations between the friction factor and the flow rate: **a** for NTK clay; **b** for HWL clay

The average root mean square error was 0.55 mm and 0.28 mm for NTK and WHL specimens, respectively.

#### 3.2 Relationship between friction factor and hole diameter in the HET

The  $\mu$ CT-scan measurements of the hole diameter at different time steps during the HET allowed calculating the friction factor using Eq. 2 and therefore investigating the evolution of the friction factor in the HET. The relationship between the friction factor and the hole diameter for the NTK clay and the HWL clay is shown in Fig. 10. The friction factor was calculated for two cases (i) considering the local head losses and (ii) without considering the local head losses according to Wan and Fell [21]. For both cases, the friction factor exhibited a linear correlation with the hole diameter with high coefficients of determination  $R^2$  (Fig. 10). However, the friction factor calculated without considering the local head losses was more than twice as high as the friction factor calculated considering local head losses.

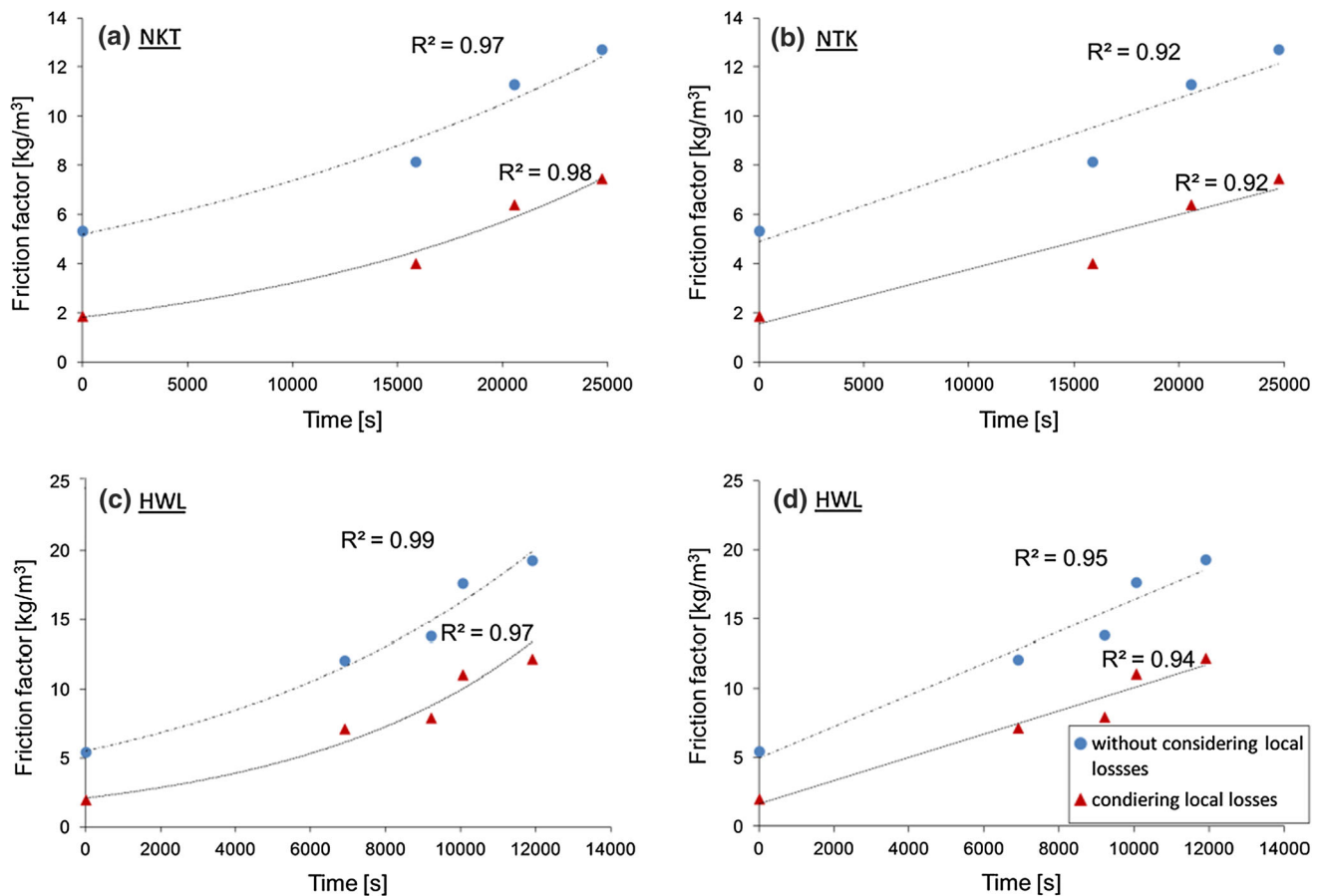


Fig. 12 Correlations between the friction factor and time: **a, b** for NTK clay specimen; **c, d** for HWL clay specimen

### 3.3 Relationship between friction factor and flow rate in the HET

Fitting a linear trendline for friction factor and flow rate, relatively high  $R^2$  can be obtained (Fig. 11). However, considering  $R^2$ , the friction factor correlates linearly with the hole diameter better than the flow rate. These results agree well with the finding of Lim [10]. In fact, a logarithmic trendline with  $R^2$  of 0.96–0.98 fits the friction factor and the flow rate data better than a linear trendline (Fig. 11).

### 3.4 Relationship between friction factor and time in the HET

By plotting the friction factor versus time, an exponential trendline can be fitted with a high  $R^2$  (Fig. 12a, c). Fitting a linear trendline to the data showed slightly lower  $R^2$  than in the case of the exponential trendline (Fig. 12b, d). It is to be noted that there were no data around the first half duration of the test except at  $t = 0$ . In this period, there was a very small increase in the flow rate with time, therefore, no  $\mu$ CT-scans were carried out. Wahl et al. [20] found a

general linear trend between friction factor and time but with a low  $R^2$ . In contrast, Lim [10] found that the friction factor does not correlate with time at all. Both Lim [10] and Wahl et al. [20] used the initial and the final data of several HETs (different specimens) to study the relation between the friction factor and time. This results in a high scatter of the data as the erosion process in different specimens could be different due to, for example, the preparation of the specimens. The analysis of the HET analysis using exponential and linear relation between the friction factor and time is presented in Sect. 4. Analysing the HET using an exponential relation between friction factor and time showed significantly higher correlation between erosion rate and hydraulic shear stress than the analysis assuming that the friction factor varies linearly with time (Fig. 16).

### 3.5 Relationship between flow rate and hole diameter

The results of the HETs and the  $\mu$ CT-scans for both clay types showed a linear correlation between the flow rate and the hole diameter in the range of the measured diameters (Fig. 13). However, it can be noted that the first points in



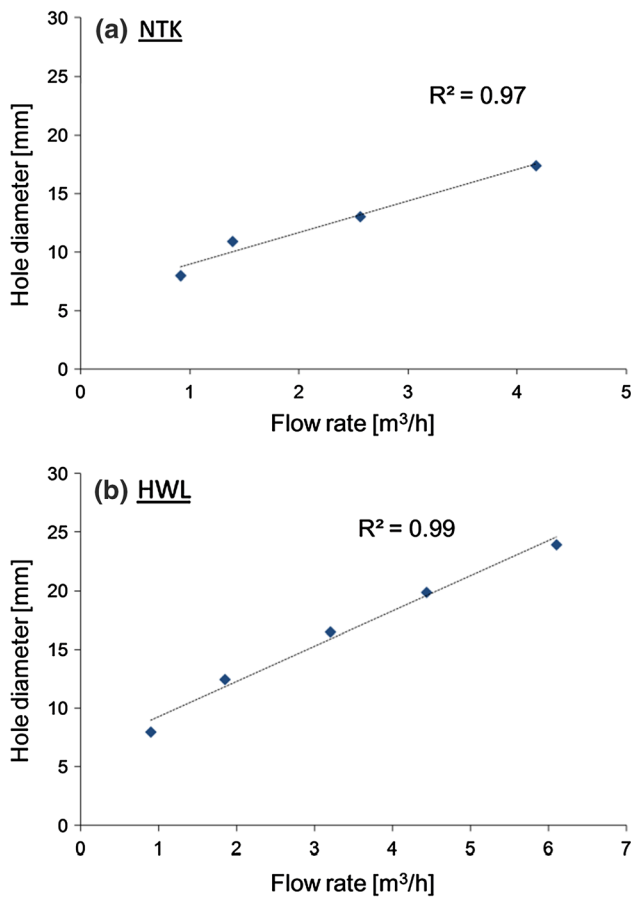


Fig. 13 Variation of the hole diameter with the flow rate: **a** for NTK clay; **b** for HWL clay

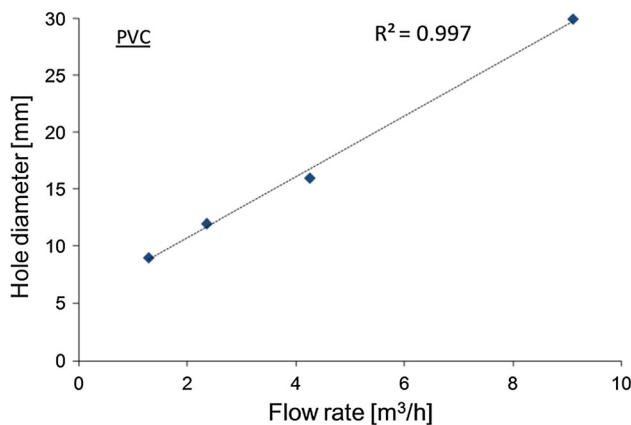


Fig. 14 Variation of the hole diameter with the flow rate for in the HETs with PVC specimens

Fig. 13a, b are slightly below the line of best-fit, indicating a slightly higher flow rate than that estimated with the line of best-fit. This can be attributed to the smooth sidewalls of the hole at the beginning of the test due to the preparation of the hole with the copper pipe.

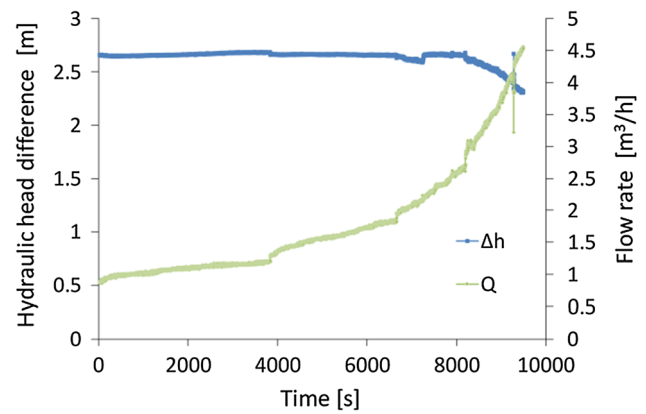


Fig. 15 Flow rate and hydraulic head difference in the HET

The relationship between the hole diameter and the flow rate was further investigated using the PVC specimens. The results of the HETs with the PVC specimens confirmed the linear variation of the flow rate with the hole diameter in the range of the tested hole diameters (Fig. 14).

#### 4 Proposed method for interpretation of the HET

A simplified interpretation method of the HET on high plastic clay is presented. The proposed interpretation method is based on the linear correlation between the hole diameter and the flow rate addressed in Sec. 3.4. Since the initial and final hole diameters in the HET are known, the hole diameter at time  $t$  ( $\phi_t$ ) can be calculated using the flow rate as given in Eq. 8.

$$\Phi_t = \Phi_i + \left( \frac{\Phi_f - \Phi_i}{Q_f - Q_i} \right) (Q_t - Q_i) \quad (8)$$

The initial hole diameter  $\phi_i$  is the diameter of the copper tube used to prepare the hole in the specimen (8 mm). The final hole diameter  $\phi_f$  can be measured at the end of the test using a plaster cast of the hole. Since the flow rate  $Q_t$  is measured continuously during the HET, the hole diameter  $\phi_t$  can be calculated at any time during the test. Accordingly, the erosion rate  $\dot{\epsilon}$  (m/s) can be calculated as the change of the hole diameter with time. Using the hole diameter, the local head losses can be calculated and therefore the effective hydraulic head difference can be obtained using Eq. 5. Ultimately, the hydraulic shear stress is calculated using Eq. 1 and the relationship between the erosion rate and the hydraulic shear stress can be established. In the proposed method there is no need to use Eq. 2 with the impeded assumptions regarding the relationship between the friction factor and hole diameter, flow rate or time.

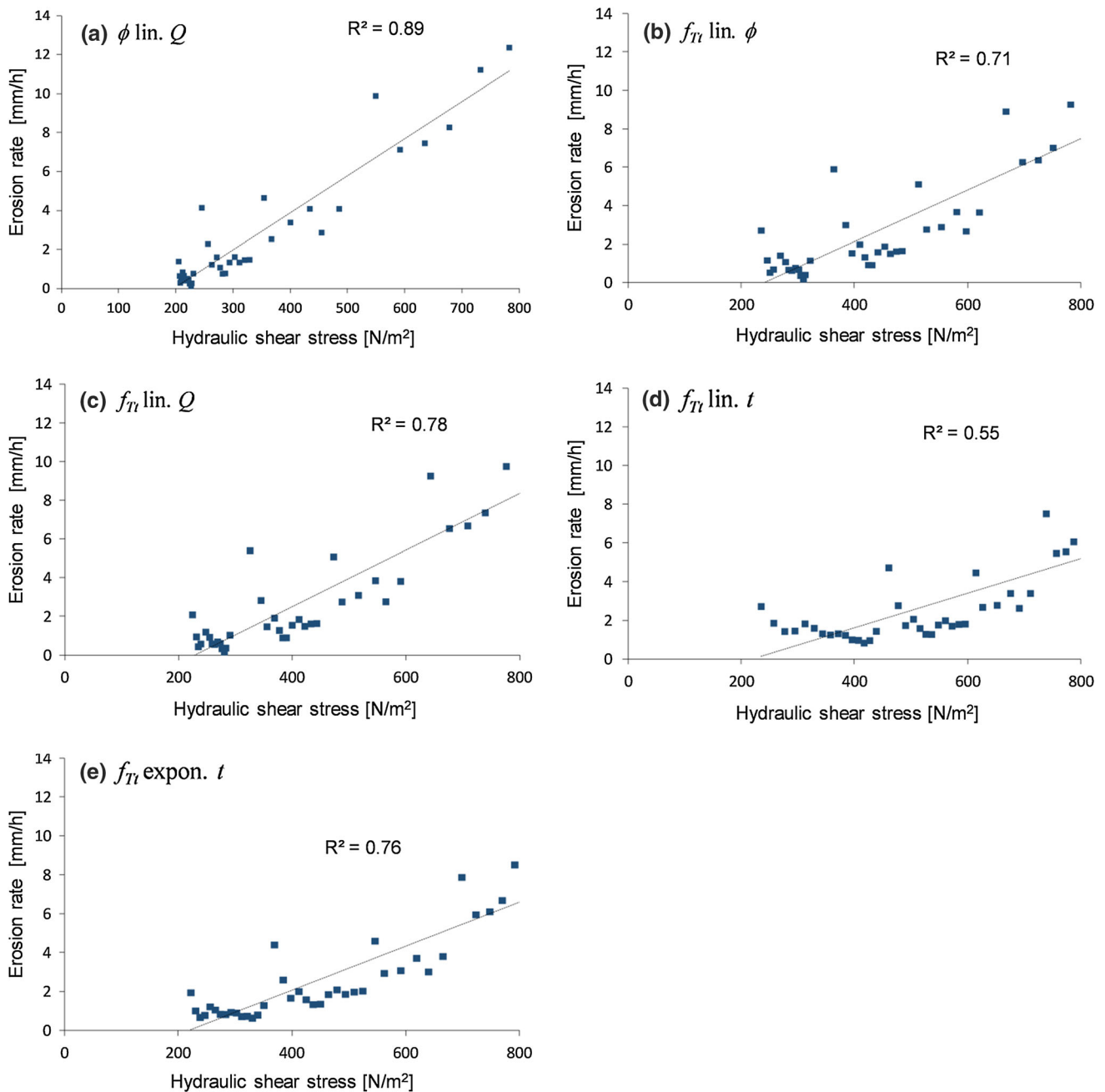


**Fig. 16** Erosion rate and hydraulic shear stress using different HET analysis methods: **a** proposed method ( $\phi$  varies linearly with  $Q$ ); **b**  $f_{Tl}$  varies linearly with  $\phi$ ; **c**  $f_{Tl}$  varies linearly with  $Q$ ; **d**  $f_{Tl}$  varies linearly with  $t$ ; **e**  $f_{Tl}$  varies exponentially with  $t$

To compare the results of the proposed analysis method and previous analysis methods of Wan and Fell [21] and Lim [10], one HET was carried out on NTK clay. The flow condition in the test was turbulent and the local head losses were considered in the analysis of the HET. The hydraulic head difference between upstream and downstream the specimen ( $\Delta h$ ) and the flow rate ( $Q_t$ ) during the HET test are shown in Fig. 15. The erosion rate and the hydraulic shear stress calculated using the proposed method are shown in Fig. 16a. The results of the HET considering that

the friction factor varies linearly with the flow rate or with the hole diameter are shown in Fig. 16b, c, respectively. The analysis using the assumption of Wan and Fell [21] that the friction factor varies linearly with time is shown in Fig. 13d. The correlation between the erosion rate and the hydraulic shear stress using exponential relation between the friction factor and time was higher than the one using the aforementioned assumption of Wan and Fell [21] and Lim [10].

**Table 4** Hole erosion test results using different analysis methods

Analysis method	$\tau_c$ [N/m <sup>2</sup> ]	$I$ [-]
Proposed method $\phi$ varies linearly with $Q$	191.8	4.99
Lim [10] $f_t$ varies linearly with $\phi$	238.4	5.10
Lim [10] $f_t$ varies linearly with $Q$	225.0	5.14
Wan and Fell [20] $f_t$ varies linearly with $t$	216.1	5.32
$f_t$ varies exponentially with $t$	215.6	5.21

The proposed analysis method showed the highest  $R^2$  (Fig. 16a) and the lowest critical shear stress and erosion rate index (Table 4). Considering the investigation of the sealing clay resistance against erosion, the new analysis method is recommended, since it provides conservative erosion parameters of the soil, i.e. lowest critical shear stress and erosion rate index. All analysis methods resulted in almost the same erosion rate index and therefore the same classification of the soil as extremely low erodible according to the classification of Wan and Fell [21].

## 5 Conclusion

Micro-computed X-ray tomography ( $\mu$ CT) was successfully employed to measure the hole diameter inside the specimen at different time intervals during the HET. The results of the  $\mu$ CT-analysis directly at the specimen showed a good agreement with results on a plaster cast of the hole determined using a photogrammetric 3D scanner confirming the accuracy of capturing the hole geometry by the  $\mu$ CT-scan. HETs were combined with  $\mu$ CT-scans, to investigate the relations between the friction factor and the hole diameter, flow rate and time. The friction factor was calculated by combining the measured head difference and the flow rate measured in the HET together with the measured hole diameter from the  $\mu$ CT-scan. The friction factor during the HET correlates linearly with the hole diameter. A logarithmic trendline fits the friction factor and the flow rate data better than a linear trendline. Moreover, an exponential relation between friction factor and time was noted. Results of the  $\mu$ CT-scans and the HET data showed that the hole diameter correlates linearly with the flow rate in the range of the herein tested hole diameters. This allowed using the flow rate to estimate the hole diameter, given that the initial and the final hole diameters are known. Accordingly, a simplified method for

interpreting the HET on high plastic clay was proposed. The results of the HET analysis using the proposed and previous analysis methods of Wan and Fell [21] and Lim [10] were compared. The proposed method showed the highest correlation between the erosion rate and the hydraulic shear stress and the lowest critical shear stress.

**Authors' contributions** All authors contributed to the study conception and design. Material preparation, data collection and analysis were performed by [BZ] and [FV]. The first draft of the manuscript was written by [BZ], and all authors commented on previous versions of the manuscript. All authors read and approved the final manuscript.

**Funding** Open Access funding enabled and organized by Projekt DEAL. This work was funded by the Federal Waterways Engineering and Research Institute (BAW) with a cooperation of Karlsruhe Institute of Technology in carrying out the  $\mu$ CT-scans.

**Availability of data and material** Available upon request.

**Code availability** Not applicable.

## Declarations

**Conflicts of interest** The authors have no financial or proprietary interests in any material discussed in this article.

**Supplementary Information** The online version contains supplementary material available at <https://doi.org/10.1007/s11440-022-01606-5>.

**Open Access** This article is licensed under a Creative Commons Attribution 4.0 International License, which permits use, sharing, adaptation, distribution and reproduction in any medium or format, as long as you give appropriate credit to the original author(s) and the source, provide a link to the Creative Commons licence, and indicate if changes were made. The images or other third party material in this article are included in the article's Creative Commons licence, unless indicated otherwise in a credit line to the material. If material is not included in the article's Creative Commons licence and your intended use is not permitted by statutory regulation or exceeds the permitted use, you will need to obtain permission directly from the copyright holder. To view a copy of this licence, visit <http://creativecommons.org/licenses/by/4.0/>.

## References

- Banasiak R, Verhoeven R (2008) Transport of sand and partly cohesive sediments in a circular pipe run partially full. *J Hydraul Eng* 134(2):216–224
- Bonelli S (ed) (2013) Erosion in geomechanics applied to dams and levees. Civil engineering and geomechanics series. ISTE Ltd, London, Hoboken, NJ
- Bonelli S (2019) The hole erosion test: state of the art, state of practise and open questions. In: EWG-IE 27th Annual Meeting
- Bonelli S, Brivois O, Borghi R et al (2006) On the modelling of piping erosion. *Comptes Rendus Mécanique* 334(8–9):555–559
- Fattahi SM, Soroush A, Shourijeh PT (2017) The hole erosion test. a comparison of interpretation methods. *Geotech. Test. J* 40(3):20160069. Doi: <https://doi.org/10.1520/GTJ20160069>

6. Haghghi I, Chevalier C, Duc M et al (2013) Improvement of hole erosion test and results on reference soils. *J Geotech Geoenviron Eng* 139(2):330–339
7. Hanson GJ, Simon A (2001) Erodibility of cohesive streambeds in the loess area of the midwestern USA. *Hydrol Process* 15(1):23–38. <https://doi.org/10.1002/hyp.149>
8. Hark M (2018) A modified hole-erosion-test on high plastic clay with different soil structure. In: *Scour and Erosion IX*. CRC Press, p 107
9. Khoshghalb A, Nobarinia M, Stockton J et al (2021) On the effect of compaction on the progression of concentrated leaks in cohesive soils. *Acta Geotech* 16(5):1635–1645
10. Lim SS (2006) Experimental investigation of erosion in variably saturated clay soils. Dissertation, University of New South Wales
11. Lüthi M (2011) A modified hole erosion test (HET-P) to study erosion characteristics of soil, University of British Columbia
12. Lüthi M, Fannin RJ, Millar RG (2012) A Modified hole erosion test (HET-P) device. *Geotech Test J* 35(4):104336. <https://doi.org/10.1520/GTJ104336>
13. Marot D, Regazzoni P-L, Wahl T (2011) Energy-based method for providing soil surface erodibility rankings. *J Geotech Geoenviron Eng* 137(12):1290–1293. [https://doi.org/10.1061/\(ASCE\)GT.1943-5606.0000538](https://doi.org/10.1061/(ASCE)GT.1943-5606.0000538)
14. Mercier F, Bonelli S, Golay F et al (2015) Numerical modelling of concentrated leak erosion during hole erosion tests. *Acta Geotech* 10(3):319–332
15. Otsu N (1979) A threshold selection method from gray-level histograms. *IEEE Trans Syst man Cybern* 9(1):62–66
16. Reiffsteck P, Pham T L, Vargas R, Paihua S (2006). Comparative study of superficial and internal erosion tests. In: 3rd international conference on scour and erosion. CURNET, Gouda, The Netherlands, pp 571–575
17. Říha J, Jandora J (2015) Pressure conditions in the hole erosion test. *Can Geotech J* 52(1):114–119. <https://doi.org/10.1139/cgj-2013-0474>
18. Schindelin J, Arganda-Carreras I, Frise E et al. (2012) Fiji. An open-source platform for biological-image analysis. *Nature Methods* 9(7):676–682
19. Schneider CA, Rasband WS, Eliceiri KW (2012) NIH Image to ImageJ. 25 years of image analysis. *Nature Methods* 9(7):671–675
20. Wahl TL, Regazzoni PL, Erdogan Z (2008) Determining erosion indices of cohesive soils with the hole erosion test and jet erosion test. US Department of Interior, Bureau of Reclamation, Technical Service Centre
21. Wan C, Fell R (2004) Investigation of rate of erosion of soils in embankment dams. *J Geotech Geoenviron Eng* 130(4):373–380
22. White FM (2011) *Fluid mechanics*, 7th edn. McGraw-Hill, New York
23. Xie L, Liang X, Su T-C (2018) Measurement of pressure in viewable hole erosion test. *Can Geotech J* 55(10):1502–1509. <https://doi.org/10.1139/cgj-2017-0292>
24. Yalin MS (1972) *Mechanics of sediment transport*, 1st edn. Pergamon Press, Oxford

**Publisher's Note** Springer Nature remains neutral with regard to jurisdictional claims in published maps and institutional affiliations.